The "shuttle" mechanism of the electron transport by the ruthenium(II) bipyridyl complex-modified bovine adrenodoxin in the steroid hydroxylase: Crystal structure and intramolecular electron transfer
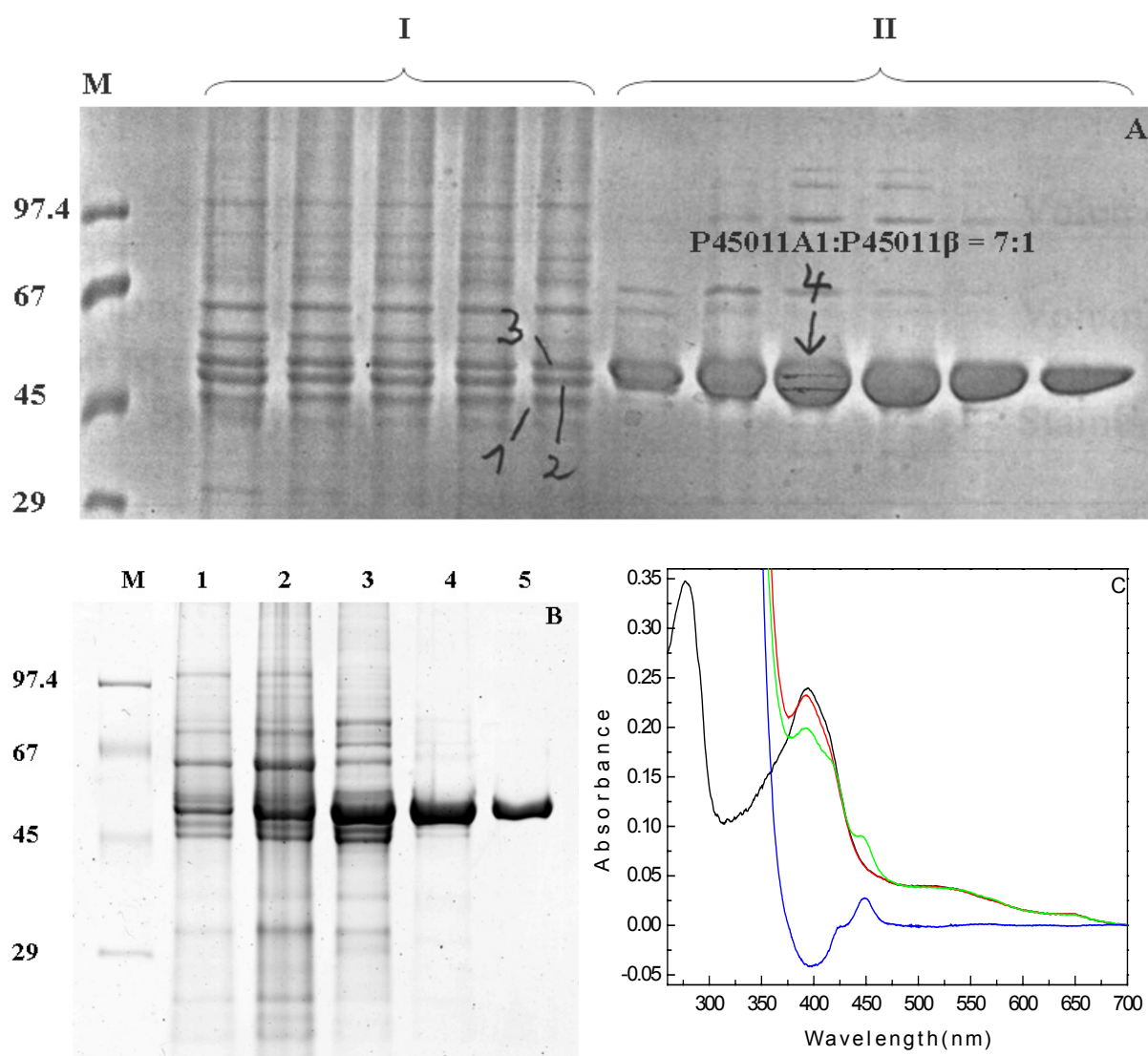
64

2.2 Results

2.2.1 Native side-chain cleavage cytochrome P450

Mitochondrial $P450_{scc}$ was purified according to Scheme B.1. Contaminants after a double $AmSO_4$ fractionation were removed by further purification on Cholate-Sepharose 4B (Figure 2.2.1.1.A). Upon loading of a Cholate-Sepharose 4B column and its further washing, $P450_{scc}$ was absorbed as a dark red band, while $P45011\beta$[19] and some other mitochondrial proteins were washed out. Some desorption of $P450_{scc}$ was also observed (Figure 2.2.1.1.A). Remaining proteins after elution of $P450_{scc}$ from the Cholate-Sepharose column were removed after Adx-Sepharose 4B, and Superdex™ 200 (Figure 2.2.1.1.B).

Most of the purified protein material showed an electrophoretic mobility corresponding to $P450_{scc}$. The obtained preparations of $P450_{scc}$ exhibited one band under 12% SDS-PAGE after gel filtration with a molecular weight of around 56 kDa (Figure 2.2.1.1.B). A spectrophotometric analysis of the eluted fractions after different chromatography steps showed that material contained also a denaturized protein, cytochrome P420. This can be seen in Figure 2.2.1.1.C where in the oxidized spectrum of $P450_{scc}$ a small shoulder at 420 nm is present. Nevertheless, most of the protein was purified as a high-spin oxidized hemoprotein, which exhibits characteristic absorption maxima at 280 nm, 393 nm, 526 nm, and 645 nm (Figure 2.2.1.1.C). The A_{393}/A_{418} ratio was 1.3-1.5, indicating that isolated protein is present in a complex with the endogenous cholesterol [Horie & Watanabe, 1975]. Reduction of $P450_{scc}$ with sodium dithionite changed the absorption maxima shifting them to 417 nm and 548 nm. The spectrum of the carbon monoxide-complexed with the heme group of the reduced cytochrome showed the typical peak at 450 nm (Figure 2.2.1.1.C).

The isolated $P450_{scc}$ was judged homogeneous based on the ratio A_{393}/A_{280} of 0.9 and a specific content of $P450_{scc}$ (300-400 nmol from 5 kg of adrenal glands).

---

[19] It is always co-purified with $P450_{scc}$.

The "shuttle" mechanism of the electron transport by the ruthenium(II) bipyridyl complex-modified bovine adrenodoxin in the steroid hydroxylase: Crystal structure and intramolecular electron transfer

65

Figure 2.2.1.1 Properties of bovine mitochondrial P450$_{scc}$. A. 12% SDS-PAGE during loading and washing of Cholate Sepharose 4B (I) and then eluting P450$_{scc}$ (II) from the column. Single bands are 3-β-hydroxysteroid dehydrogenase (1), P45011β (2), P450$_{scc}$ (3 and 4), as analyzed by mass spectrometry, which was performed by Dr. E.-C. Müller. M – molecular weight marker. B. 12% SDS-PAGE of bovine P450$_{scc}$ purified from mitochondria: (lane 1) 27-43% of ASP; (lane 2) 43-40% of ASP; (lane 3) Cholate-Sepharose 4 B; (lane 4) Adx-Sepharose 4B; (lane 5) gel filtration on a Superdex™ 200. C. UV-visible spectra of P450$_{scc}$: oxidized high-spin cytochrome (black); dithionite reduced (red); dithionite reduced and treated with CO (green); CO difference spectrum (blue).

Further properties of native P450$_{scc}$ were observed. The purified enzyme can be stored at -20 °C in 50 mM potassium phosphate buffer containing 1 M KCl, 0.3% sodium cholate, and 20% glycerol for at least 2 months without any loss of activity or changes of electrophoretic properties. Flash-freezing of the protein in liquid nitrogen and subsequent storage at -70 °C

The "shuttle" mechanism of the electron transport by the ruthenium(II) bipyridyl complex-modified bovine adrenodoxin in the steroid hydroxylase: Crystal structure and intramolecular electron transfer

66

preserved the protein activity for more than 2 months. However, repeated freezing and thawing as well as storage at 4 °C increased the amount of degraded enzyme.

The side-chain activity of $P450_{scc}$ was not carried out in this thesis. The activity of the enzyme was just investigated in a NADPH-induced reduction assay within the reconstituted steroid hydroxylase system (see below).

2.2.2 Recombinant bovine adrenodoxin reductase

The protein was co-expressed with the Hsp60-chaperone system to provide better folding of the reductase. High-level coexpression of GroEL and GroES was observed in 12% SDS-PAGE (Figure 2.2.2.1.A). GroEL and GroES as single subunits [Martin et al., 1993] showed molecular weights of 60 and 10 kDa, respectively. Their separation as well as the removal of other contaminants from AR was completed with $AmSO_4$ precepitation and subsequent affinity chromatography steps on Adx-Sepharose 4B and 2',5'-ADP-Sepharose 4B. AR was obtained with high purity index $A_{280}/A_{450} = 6.5$-7.0. The oxidized protein solution had yellow color and exhibited one maximum in the UV region at 270 nm and two broad maxima in the visible range at 360 and 450 nm (Figure 2.2.2.1.B). These spectral characteristics in the visible region are common among known FAD-containing proteins and originate from the presence of FAD co-factor. The protein was stable and active over a long period of time if the protein solution was stored in small glycerol stock aliquots at -70 °C.
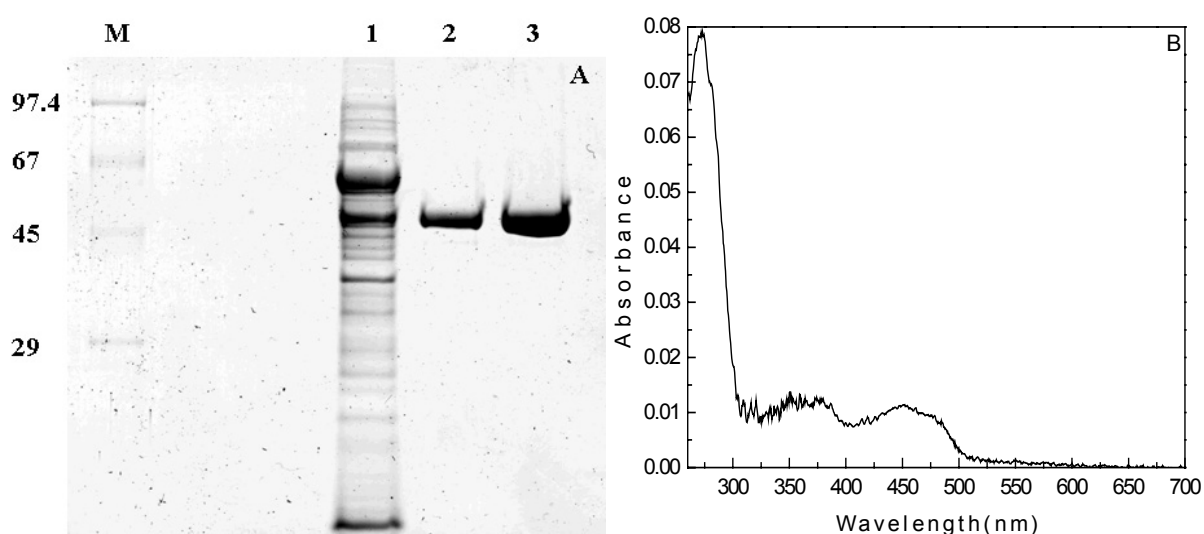
Figure 2.2.2.1 Properties of recombinant AR. A. 12% SDS-PAGE of bovine recombinant AR. 1. soluble fraction after FP; 2. Adx-Sepharose 4B; 3. 2',5'-ADP-Sepharose 4B. M − molecular weight marker. B. UV-vis absorption spectrum of recombinant AR.

The "shuttle" mechanism of the electron transport by the ruthenium(II) bipyridyl complex-modified bovine adrenodoxin in the steroid hydroxylase: Crystal structure and intramolecular electron transfer
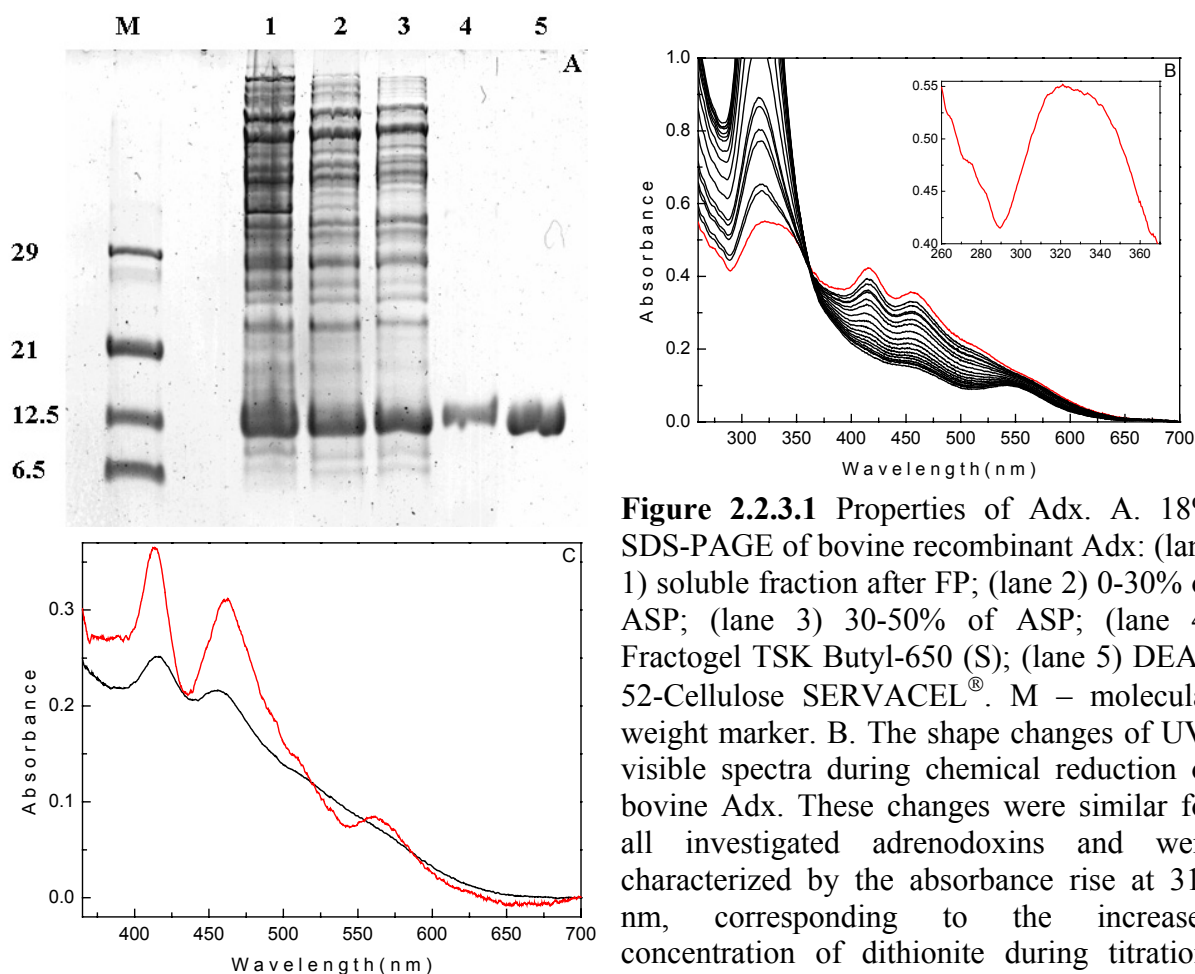
67

2.2.3 Recombinant bovine wild-type Adx

In this work recombinant wild-type Adx was purified mostly for comparative investigations with other adrenodoxins, Adx(1-108), and Ru(bpy)$_2$(mbpy)-Adx(1-108). Adx(WT) was also used in coupling to CNBr-activated Sepharose 4B, which was used for purification of AR and P450$_{scc}$.

Since Adx(WT) did not carry any affinity tags, its purification was started with fractionated ASP. This procedure helped to remove about 40-50% of the accompanying proteins. In the process of loading and washing the Fractogel TSK Butyl-650 (S) and DEAE 52-Cellulose SERVACEL$^®$ columns, remaining contaminants were removed and Adx was purified. Spectrophotometric analysis of the eluted fractions showed drastic increase of the A$_{414}$/A$_{276}$ ratio from 0.4-0.45 after Fractogel TSK Butyl-650 (S) to 0.89-0.9 after DEAE 52-Cellulose SERVACEL$^®$. After gel filtration it became 0.93. In Figure 2.2.3.1.A a single band at 13-14 kDa after the last chromatography indicates that purified Adx is homogeneous.

A solution of oxidized Adx(WT) was reddish-brown and had characteristic absorption maxima at 414 nm and 455 nm with a small shoulder at 518 nm in the visible region (Figure 2.2.3.1.B). The ultraviolet absorption spectrum displays a broad maximum at 320 nm which appears to consist of two peaks and three maxima at 259 nm, 265 nm, and 276 nm with two shoulders at 253 nm and 283 nm (inset of Figure 2.2.3.1.B). These main three maxima at 320 nm, 414 nm, and 455 nm are a characteristic feature of native Adx, which also indicates proper folding and presence of the [2Fe-2S] cluster. Some improvement in resolution of the solution spectrum was obtained at the temperature of liquid nitrogen (Figure 2.2.3.1.C). This was also earlier observed by *Palmer et al.* [Palmer et al., 1967].

The spectra of Adx reduced either by dithionite or by NADPH plus AR exhibit a distinct feature (Figure 2.2.3.1.B): The absorption maxima at 320 nm, 414 nm, and 455 nm greatly decrease, although they do not disappear completely. A new maximum appears at 540 nm.

The "shuttle" mechanism of the electron transport by the ruthenium(II) bipyridyl complex-modified bovine adrenodoxin in the steroid hydroxylase: Crystal structure and intramolecular electron transfer

68

Figure 2.2.3.1 Properties of Adx. A. 18% SDS-PAGE of bovine recombinant Adx: (lane 1) soluble fraction after FP; (lane 2) 0-30% of ASP; (lane 3) 30-50% of ASP; (lane 4) Fractogel TSK Butyl-650 (S); (lane 5) DEAE 52-Cellulose SERVACEL®. M – molecular weight marker. B. The shape changes of UV-visible spectra during chemical reduction of bovine Adx. These changes were similar for all investigated adrenodoxins and were characterized by the absorbance rise at 312 nm, corresponding to the increased concentration of dithionite during titration. The changes were also followed by the absorbance decrease at 414 nm, corresponding to the reduction of the [2Fe-2S] cluster. The inset represents a close-up view of the oxidized spectrum of Adx in the range between 260 nm and 370 nm. C. Absorption spectra of oxidized bovine Adx at room temperature (293 K) (black) and 80 K (red).

2.2.4 Recombinant bovine Adx(N-6×His tag/Xa/1-108) and Adx(1-108)

The total yield of pure Adx(N-6×His tag/Xa/1-108) ($A_{414}/A_{276} = 0.93$) was 6-7 μmol from 8 L culture. The protein spectral and electrophoretic mobility properties did not differ from those of Adx (Figure 2.2.3.1).

Before and all through the cleavage of the 6×His tag of Adx(N-6×His tag/Xa/1-108) aliquots were taken and analyzed by 18% SDS-PAGE. In addition to a major band at 12.5 kDa, two other prominent bands below 29 kDa and at 21 kDa were observed before the cleavage

reaction was started. Whereas the first band (29 kDa) (Figure 2.2.4.1, lane 1) may correspond to a dimer of Adx at concentrations higher than 1 mM (used in the cleavage reaction with Xa), the nature of the second band (21 kDa) is not clear. These bands did not disappear completely after cleavage of the tag (Figure 2.2.4.1, lane 3). However, decreasing the initial Adx concentration before cleavage with Xa led to disappearance of these bands (Figure 2.2.4.1, lane 4). It is good to see that after cleavage of the tag Adx migrates below a band of the original mutant (Figure 2.2.4.1, lane 2 and lane 3).
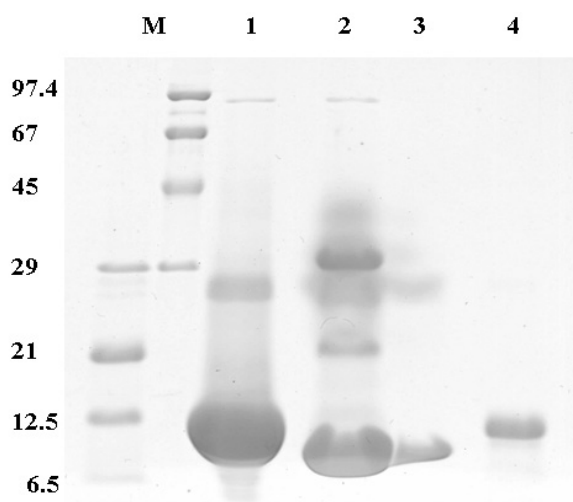

Figure 2.2.4.1 Cleavage of the N-6×His tag of Adx(N-6×His tag/Xa/1-108). (lane 1) Adx(N-6×His tag/Xa/1-108) at $\geq$ 1 mM concentration; (lane 2) after overnight incubation with Xa and before applying a reaction solution to Xarrest™ agarose. Xa migrated in 18% SDS-PAGE gel as two bands with molecular weights of 34 kDa and 29 kDa (according to the Novagen standard cleavage protocol); (lane 3) after recovery of modified Adx; (lane 4) Adx(N-6×His tag/Xa/1-108) at $\leq$ 1 mM concentration. M – molecular weight marker.

Recovered from a Xarrest™ agarose column, Adx(1-108) did not show any affinity to a Ni-NTA agarose and it was pure from Xa (Figure 2.2.4.1, lane 3). After additional gel filtration, modified Adx had an A_{414}/A_{276} ratio of 0.9, and was subjected to a mass spectrometry analysis.

2.2.5 Ru(bpy)$_2$(mbpy)-Adx(1-108) complex

During addition of the DMSO-dissolved Ru(bpy)$_2$(Br-mbpy)(PF$_6$)$_2$ to Adx(1-108), the solution of the protein turned a little cloudy. This may arise from partial destabilization and denaturation of the protein with loss of enzymatic activity by the organic co-solvent, DMSO. A residual amount of free non-reacted ruthenium complex was removed during injection of the whole sample (fraction 2, Figure 2.2.5.1.A). Free ruthenium complex was eluted as a single yellow band, whereas a reddish-brown band of adrenodoxin remained attached to the top of the column. Fractions with different Ru(bpy)$_2$(mbpy):Adx(1-108) ratios were eluted at 16-32% of 1 M KCl in buffer A (Figure 2.2.5.1.A). As determined from spectrophotometric measurements, only fractions 16 and 17 contained the 1:1 Ru(bpy)$_2$(mbpy)-Adx(1-108) complex, which was

The "shuttle" mechanism of the electron transport by the ruthenium(II) bipyridyl complex-modified bovine adrenodoxin in the steroid hydroxylase: Crystal structure and intramolecular electron transfer

70

obtained at 22-24% of the salt gradient. The modified protein exhibited a larger molecular weight than almost Ru(bpy)$_2$(mbpy)-free Adx(1-108) (Figure 2.2.5.1.B). The content of free Adx(1-108) which was obtained at higher salt concentration (fractions 18-20 in Figure 2.2.5.1.A) accounts for 10-20% of the total protein used in the coupling reaction.
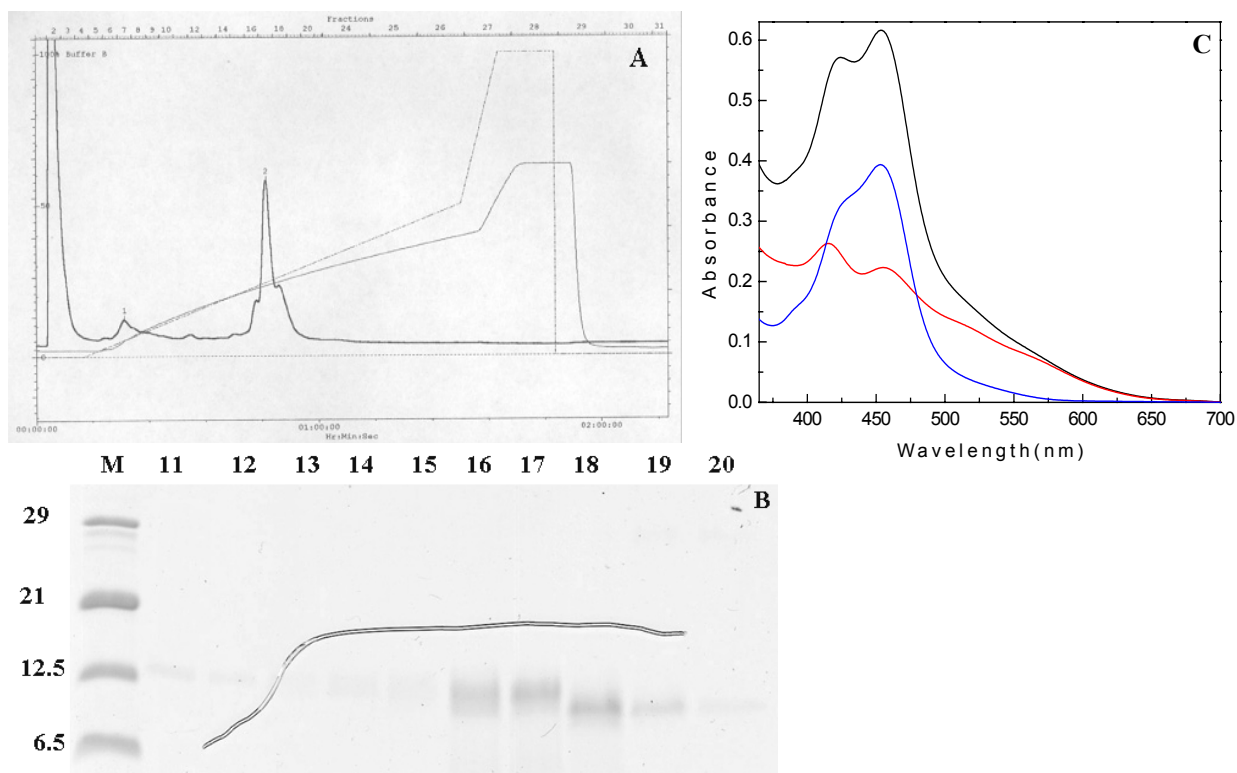

Figure 2.2.5.1 Modification of Adx(1-108) with Ru(bpy)$_2$(mbpy). A. DEAE-Bioscale Q2 elution profile. Peak 1 is for Ru(bpy)$_2$(mbpy)-Adx(1-108) complexes with molar Ru:Adx ration smal-ler than 0.5. Peak 2 contains fractions 16 and 17 with the 1:1 Ru(bpy)$_2$(mbpy)-Adx(1-108) complex. B. 18% SDS-PAGE of the colored fractions (11-20). The fraction of the non-reacted ruthenium complex was not analyzed. C. Differences in the visible spectra of the oxidized Adx(1-108) (red) and the modified Adx(1-108) (black) are due to the contribution of the ruthenium-compound spectrum (blue) in the spectrum of the protein. All spectra were obtained at different concentrations.

In Figure 2.2.5.1.C absorption spectra of uncoupled Adx(1-108), free ruthenium(II) bipyridyl complex, and Ru(bpy)$_2$(mbpy)-Adx(1-108) are shown. One main contribution of the covalently attached ruthenium moiety to the spectrum of the ferredoxin is observed in the wavelength range between 414 nm and 500 nm. This is because of the higher extinction coefficient, namely at 456 nm, for Ru(bpy)$_2$(mbpy). There is a shift of the peak at 414 nm to ~420 nm, also due to the contribution of the spectrum of the ruthenium complex.

No specific complex of Ru(bpy)$_2$(mbpy) and Adx(C95S) mutant could be purified that is taken to confirm Cys95 as the modification site. The purified 1:1 Ru(bpy)$_2$(mbpy)-Adx(1-108) complex was further analyzed by mass spectrometry to determine its molecular weight.

2.2.6 Electro-spray time-of-flight mass spectrometry data

Mass spectrometry confirmed the complete cleavage of the N-6×His tag and formation of the 1:1 Ru(bpy)$_2$(mbpy)-Adx(1-108) complex(Figure 2.2.6.1.A and 2.2.6.1.B).
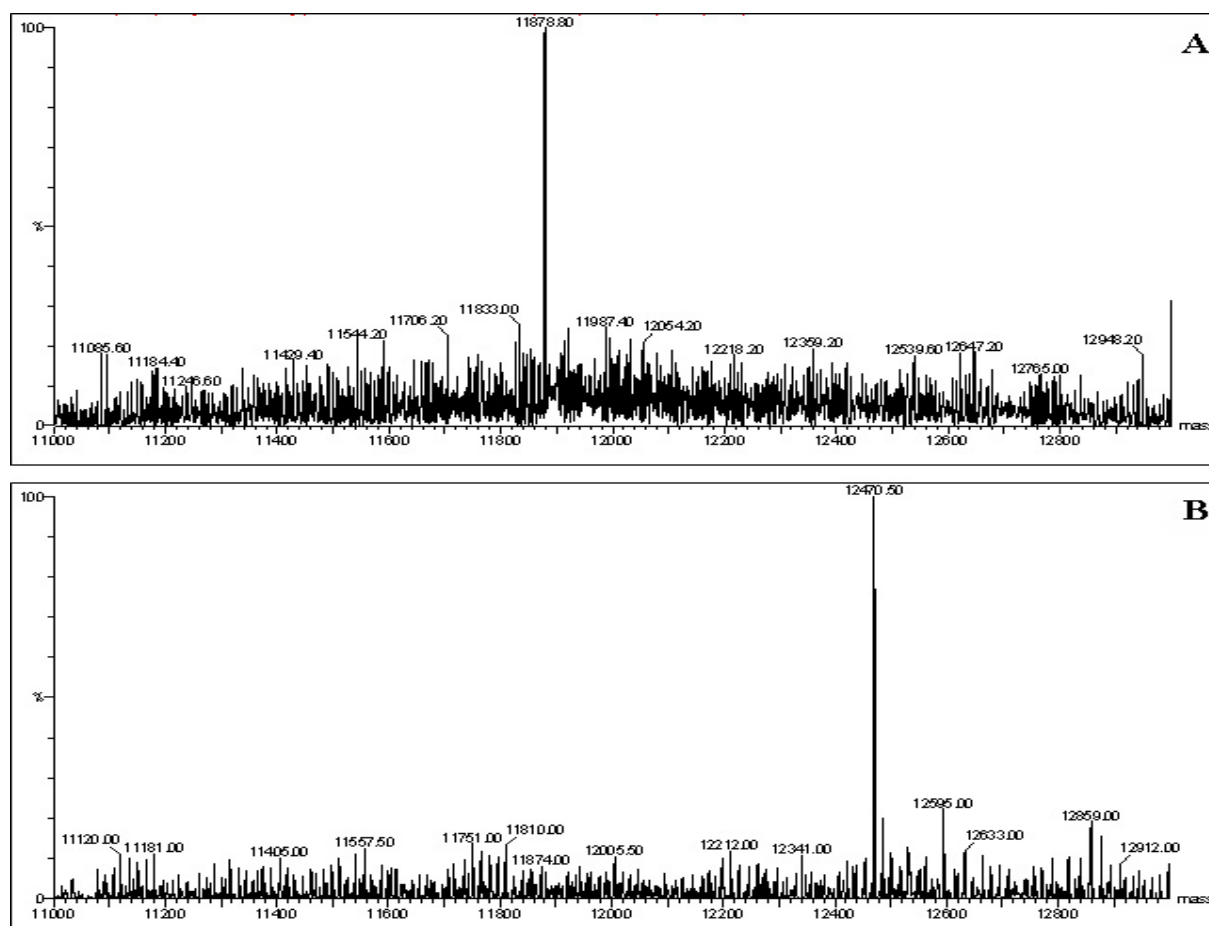

Figure 2.2.6.1 ES-TOF-MS. A. Adx(1-108) after enzymatic cleavage of the N-terminal 6×His tag. B. 1:1 Ru(bpy)$_2$(mbpy)-Adx(1-108) covalent complex.

Experimental molecular weights of 11879.0 Da (Adx(1-108)) and 12470.5 Da (Ru(bpy)$_2$(mbpy)-Adx(1-108)) are in agreement with the theoretical values, 11880.4 and 12472.04 Da, respectively, calculated without the [2Fe-2S] cluster.

The "shuttle" mechanism of the electron transport by the ruthenium(II) bipyridyl complex-modified bovine adrenodoxin in the steroid hydroxylase: Crystal structure and intramolecular electron transfer

72

2.2.7 Redox potentials

The redox potentials of Adx(WT), Adx(1-108), and Ru(bpy)$_2$(mbpy)-Adx(1-108) were measured as −282±4.5, −302±4.6, and −306±5.2 mV, respectively. The Nernst slopes for these proteins were determined: 26±1.1, 31±1.5, and 28±1.8 mV, respectively (Figure 2.2.7.1). These values are close to 30 mV, see Eqn. 2.11.2, indicating transfer of two electrons from the dye to Adx. Measuring the redox potential of P450$_{cam}$ (−312±5.8 mV) a slope of 66±2.8 mV was determined. This corresponds to 60 mV for a one-electron transfer, as expected.
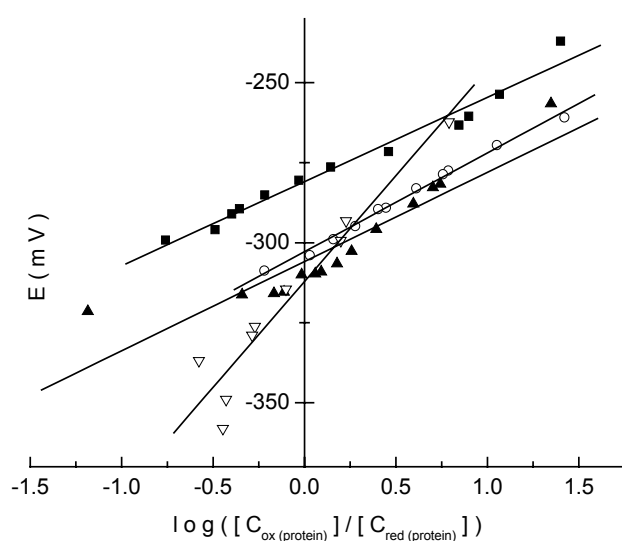
Figure 2.2.7.1 Determination of the redox potentials of adrenodoxins and P450$_{cam}$. Adx(WT) (■), Adx(1-108) (○), Ru(bpy)$_2$(mbpy)-Adx(1-108) (▲), and P450$_{cam}$ (∇). The *y* intercept of each fitting curve (solid lines) gives the redox potential of a protein. $n_{(protein)}$ for Adx and P450$_{cam}$ could be derived from the slope of every linear fit in the plot.

2.2.8 NADPH-induced reduction of P450$_{scc}$ and cytochrome *c* reduction assays

Adx(WT), Adx(1-108), and Ru(bpy)$_2$(mbpy)-Adx(1-108) were active in transporting electrons from AR to P450$_{scc}$ and from AR to cytochrome *c*. Using these assays it was also shown that purified recombinant AR is active in delivering the reducing species from NADPH to the electron carrier, Adx. The data are presented in Figure 2.2.8.1 and Table 2.2.8.1.

During P450$_{scc}$ reduction, no new spectral properties, in comparison to those displayed by Adx(WT) and Adx(1-108), were observed when Ru(bpy)$_2$(mbpy)-Adx(1-108) shuttled the electrons. Therefore, in Figure 2.2.8.1.A an experiment with Ru(bpy)$_2$(mbpy)-Adx(1-108) is shown only. Generally, as for the use of Adx(WT) and Adx(1-108) as carriers, the reduction was characterized by a peak shift from 393 nm to 417 nm. A treatment of the reduced cytochrome with CO produced a specific peak at 450 nm which was detectable for each of the three ferredoxins. Moreover, this peak could also be easily differentiated from a shoulder at 456 nm
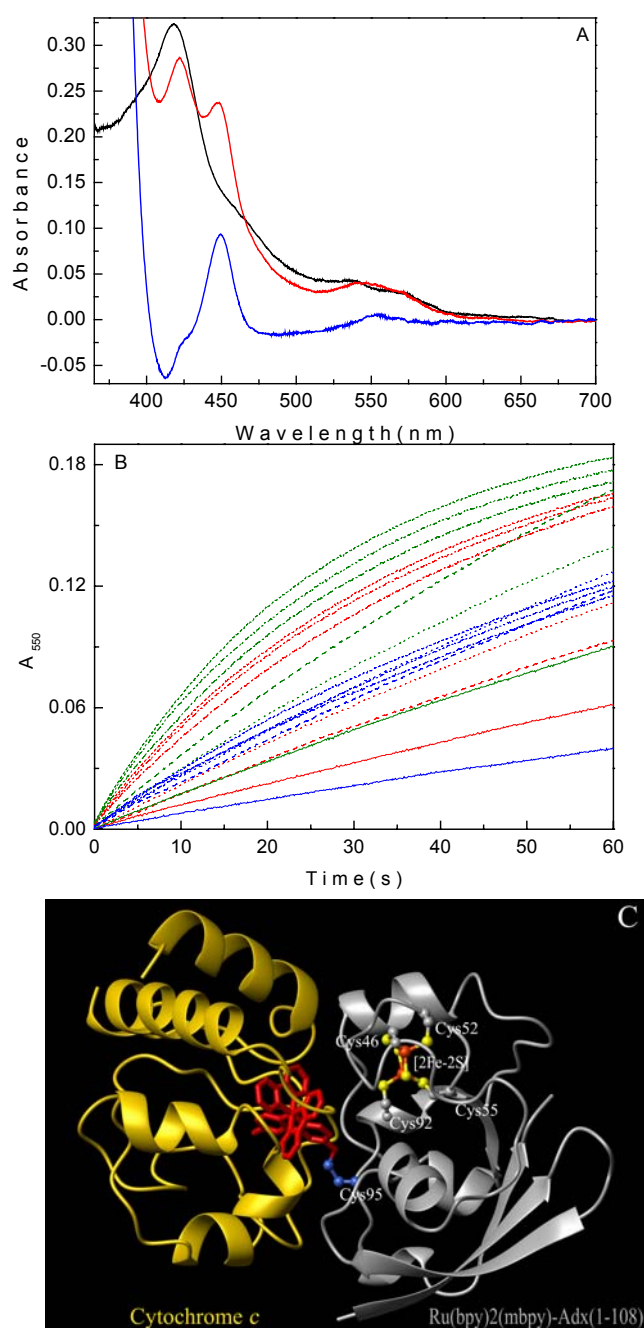
The "shuttle" mechanism of the electron transport by the ruthenium(II) bipyridyl complex-modified bovine adrenodoxin in the steroid hydroxylase: Crystal structure and intramolecular electron transfer

73

that is due to the spectral contribution of Ru(bpy)$_2$(mbpy), in case of Ru(bpy)$_2$(mbpy)-Adx(1-108). Some amount of P420 was also detectable by the presence of a small shoulder at 420 nm in the CO-difference spectrum (blue spectrum in Figure 2.2.8.1.A).

Adx(1-108) showed the fastest electron-transfer capability between the three adrenodoxins by the reduction of cytochrome *c*, whereas Ru(bpy)$_2$(mbpy)-Adx(1-108) the slowest (Table 2.2.8.1). From the calculated and compared activities it could be concluded that the specific covalent modification of Adx(1-108) may influence the protein function of an electron carrier.

Table 2.2.8.1 Cytochrome *c* reduction assay

Protein	Activity, nmoles/nmoles/min[a]
Adx(WT)	59.5±3.2[b]
Adx(1-108)	62.5±7.0
Ru(bpy)$_2$(mbpy)-Adx(1-108)	40.2±4.0

[a]Cytochrome *c* reduction was followed at 550 nm in the presence of 140 μM NADPH. [b]Standard deviations were calculated from two independent experiments, including six measurements with variable concentrations of substrates.

The "shuttle" mechanism of the electron transport by the ruthenium(II) bipyridyl complex-modified bovine adrenodoxin in the steroid hydroxylase: Crystal structure and intramolecular electron transfer

74

Figure 2.2.8.1 A. NADPH-induced reduction of P450scc. Oxidized (black) and carbon monoxide-bound form (red) spectra of the reduced P450scc when the 1:1 Ru(bpy)₂(mbpy)-Adx(1-108) complex was used as electron carrier in the reconstituted steroid hydroxylase system. CO-difference spectrum of P450scc (blue). B. Concentration dependent measurements of the kinetics of the cytochrome c reduction by adrenodoxins. Adx (red), Adx(1-108) (green), and Ru(bpy)₂(mbpy)-Adx(1-108) (blue). 0.05 (solid), 0.075 (dash), 0.1 (dot), 0.125 (dash dot), 0.15 (dash double dot), and 0.175 (short dash) µM concentrations of adrenodoxins. After 2 min all curves approached saturation indicating complete reduction of cytochrome c. C. Interaction interface between Ru(bpy)₂(mbpy)-Adx(1-108) (grey) and cytochrome c (yellow). The [2Fe-2S] cluster of Adx(1-108) is in orange-yellow ball-and-stick representation. Ru(bpy)₂(mbpy) covalently bound to Cys95 (blue) is in red stick representation. The peptide stretches of both proteins are not shown. The picture was prepared using the program MOLMOL [Koradi et al., 1996].

Since it was shown that Adx(1-108) and Ru(bpy)₂(mbpy)-Adx(1-108) have nearly identical redox potentials[20] (see above), the slowed reduction kinetics of cytochrome c by the coupled Adx may have another explanation. By molecular modeling and energy minimization for free Adx and cytochrome c and the Adx-cytochrome c complex it was shown that, in the complex with the

---

[20] The midpoint potential of adrenodoxin is a property that defines the protein function to transport electrons to the redox partners. The more negative the potential, the faster the electron transfer will occur. In case of both Adx(1-108) with -302 mV and Ru(bpy)₂(mbpy)-Adx(1-108) with -306 mV no differences in electron transfer rate should be present.

The "shuttle" mechanism of the electron transport by the ruthenium(II) bipyridyl complex-modified bovine adrenodoxin in the steroid hydroxylase: Crystal structure and intramolecular electron transfer

75

lowest energy, the peptide stretches Ile25-Asp31, Cys46-Leu50, Glu68-Glu73, and Cys92-Thr97 of Adx and Val11-Cys17, Lys27-Thr28, and Asn70-Lys86 of cytochrome c form the interface [Müller, E.-Ch. et al., 2001]. The Adx peptide stretch Cys92-Thr97 contains the Cys95 – Ru(bpy)$_2$(mbpy)-modification site, and it is good to see in Figure 3.8.1.C that the compound is at the proteins interface, and "buried" into the protein matrix of cytochrome c, as it was obtained from the least-squares fitting of the C$^\alpha$ positions of unmodified and ruthenated adrenodoxins.

2.2.9 Crystal structure of 1:1 Ru(bpy)$_2$(mbpy)-Adx(1-108)

The crystal structure of the 1:1 Ru(bpy)$_2$(mbpy)-Adx(1-108) complex was determined at 1.5 Å resolution and deposited with the PDB under the access code 2BT6.

In Figure 2.2.9.1 crystals of the covalent 1:1 Ru(bpy)$_2$(mbpy)-Adx(1-108) complex and its diffraction pattern are shown. Small, multiple crystals diffracted to 2.4 Å resolution only. Electron density was observed in the vicinity of Cys95 (Figure 2.2.9.2.A), the site at which the ruthenium complex was excepted to be covalently attached. However, no electron density for the covalent link between Cys95 and the complex was observed at 2.4 Å resolution. Using this data set, the crystal structure was refined to R/R_{free} of 23%/27% only. Refinement was terminated, because it proved impossible to build the ruthenium complex into the electron density (2.2.9.2.B). The overall B-factors of two Ru(bpy)$_2$(mbpy) moieties in the asymmetric unit of the 2.4 Å structure were high (76 Å^2).

Bigger crystals diffracted to 1.5 Å resolution. These crystals were used for data collection and solving the crystal structure of the 1:1 Ru(bpy)$_2$(mbpy)-Adx(1-108) complex.
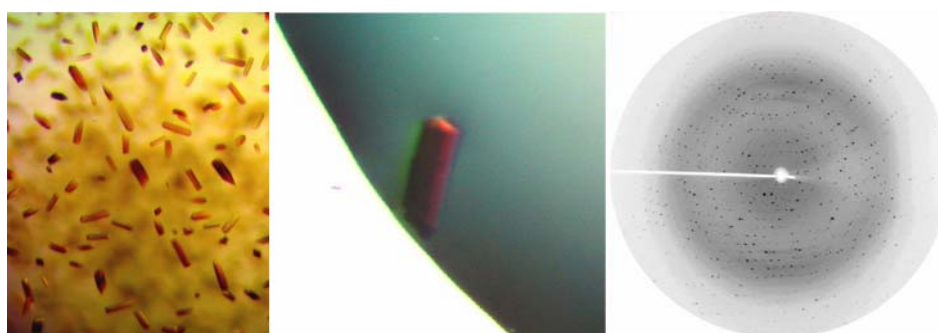
Figure 2.2.9.1 Crystallization of the Ru(bpy)$_2$(mbpy)-Adx(1-108) complex. The diffraction pattern of a big single crystal is shown.

The crystallographic data are summarized in Table 2.2.9.1. No NCS elements could be detected by self-rotation function in AMoRe. The Matthews coefficient is in the expected range

The "shuttle" mechanism of the electron transport by the ruthenium(II) bipyridyl complex-modified bovine adrenodoxin in the steroid hydroxylase: Crystal structure and intramolecular electron transfer

76

(2.71 $Å^3$/Da), when the presence of two independent protein molecules A and B in the asymmetric unit with a solvent content of 54.33% is assumed.

**Table 2.2.9.1** X-ray data collection and refinement of the Ru(bpy)$_2$(mbpy)-Adx(1-108) structure

Parameters		Values
Diffraction data[a]	Space group	P2$_1$2$_1$2$_1$
	Cell constants *a / b / c*	50.51 / 56.97 / 79.08
	Resolution (Å)	1.5
	Mosaicity (°)	0.1
	Observed / unique reflections	259,462 / 35,907
	Redundancy (all data / last shell)	7.2 / 6.2
	Completeness % (all data / last shell)	95.7 / 89.6
	R_{sym}[b] % (overall / last shell)	5.4 / 38.5
	$\langle I/\sigma(I) \rangle$ (overall / last shell)	19.1 / 4.4
Asymmetric unit	Complexes / atoms	2 / 2024
	Protein chains / residues / atoms	2 / 204 / 1868
	Iron-sulfur clusters / atoms	2 / 8
	Water molecules	215
	Ruthenium complex, chains / atoms	2 / 78
Aver. B / R-factors	Ru(bpy)$_2$(mbpy)-Adx(1-108), A / B ($Å^2$)	10.61 / 11.17
	Solvent ($Å^2$)	18.94
	R[c] / R_{free}[d]	16.67 / 19.26
r.m.s.d.	Bond distances (Å)	0.012
	Bond angles (°)	3.125

[a]using XDS. [b]$R_{sym} = \sum \left| I - \langle I \rangle \right| / \sum \left| I \right|$. [c]$R = \sum \left| F_{obs} - F_{calc} \right| / \sum \left| F_{obs} \right|$. [d]The free R factor was calculated using 5% randomly selected reflections.

Generally, molecule A of the Ru(bpy)$_2$(mbpy)-Adx(1-108) complex was better refined than molecule B in the asymmetric unit. The electron density of the N-terminal part (first 4-5 amino-acid residues) of both protein molecules was so poor that it was impossible to build them. Other residues show well-resolved $2F_o$-F_c electron density of their backbones and side chains. The residues His10, Lys24, Asp27, His62, Arg87, and Cys95 in the molecule A, and residues His62, Asp86, and Cys95 in the molecule B show additional side-chain conformations.

Prominent electron density which protrudes from the protein surface in the form of open circles, indicating the presence of aromatic rings, was observed in the vicinity of Cys95 of both Adx(1-108) molecules in the asymmetric unit (using 1.5 Å resolution data) (Figure 2.2.9.2.C). Residual difference density revealed the simultaneous binding to Adx(1-108) of the other
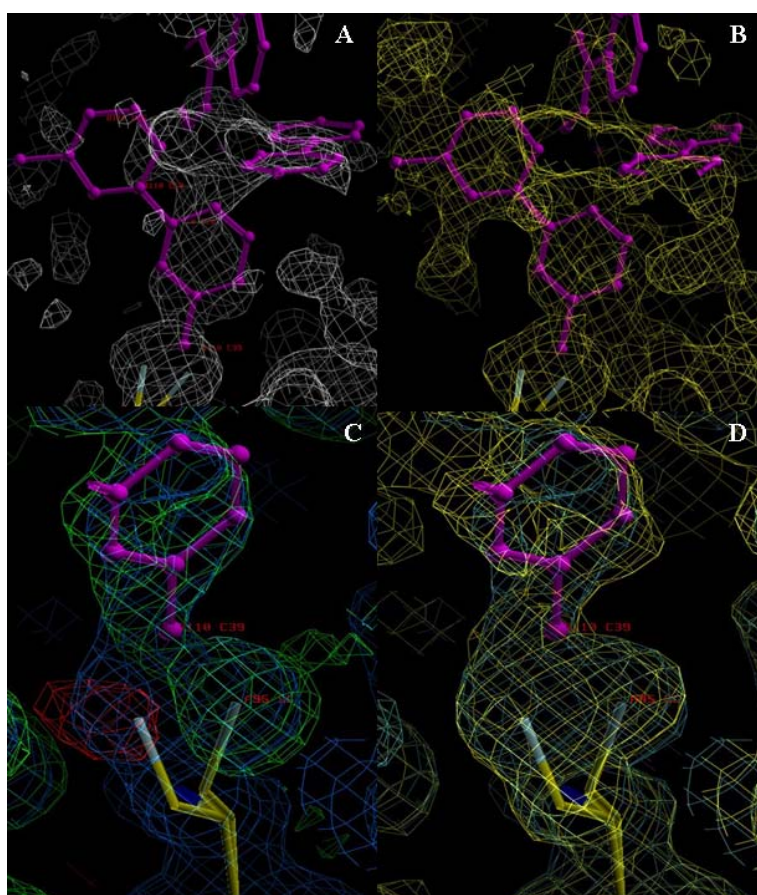
Ru(bpy)$_2$(mbpy) isomer in the crystal lattice. Clearly observed $2F_o$-F_c electron density between the C^{39} atom of the Ru(bpy)$_2$(mbpy) moiety and the side chain of Cys95 confirms the existence of the covalent link to both isomers.
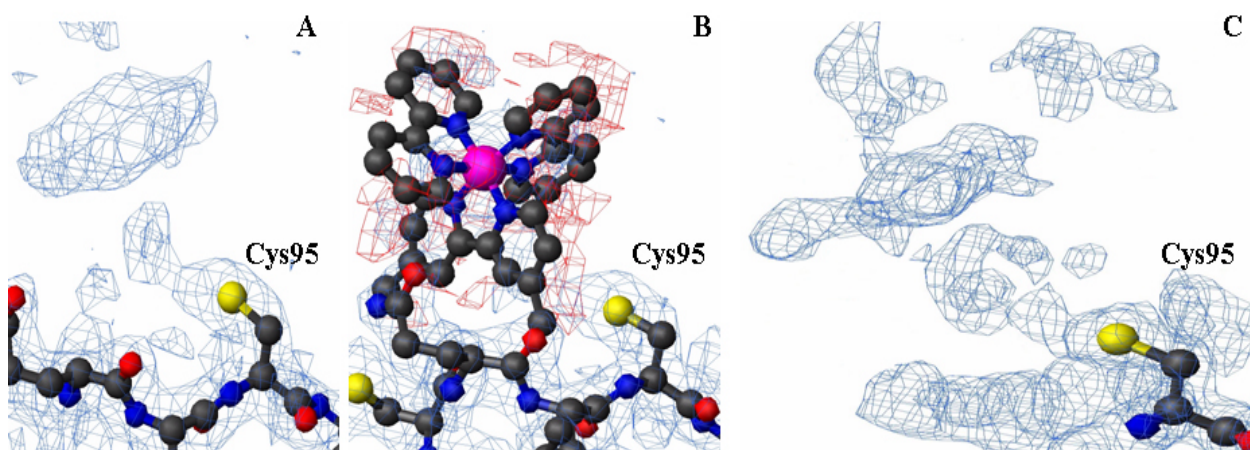
Figure 2.2.9.2 The vicinity of Cys95 of Adx(1-108) in the crystal structure of Ru(bpy)$_2$(mbpy)-Adx(1-108) complex. A. and B. The $2F_o$-F_c (blue) and F_o-F_c (red) electron densities (generated at 1σ) using 2.4 Å resolution data. A peptide chain of Adx(1-108) and Ru(bpy)$_2$(mbpy) are drawn in ball-and-stick representation. Individual atoms are: C (black), O (red), N (blue), S (yellow), and Ru (magenta). C. The $2F_o$-F_c (blue) density (generated at 1σ) of a 1.5 Å resolution data set. Cys95 is shown in ball-and-stick representation. The pictures were prepared using the program MOLMOL [Koradi et al., 1996].

With the holographic method implemented in the program EDEN [Szoke 1993] it was possible, using *a priori* real-space information and measured intensities, to generate electron density with the properties of an omit map. This helped to improve the density for the ruthenium complex by finding the correct positions of the bipyridyl ligands of the moiety (Figures 2.2.9.3.A and 2.2.9.3.B). This, together with the occupancy for Δ- and Λ-isomer in chain A set to 0.4, and the occupancy in chain B set to 0.4 (Δ) and 0.6 (Λ), helped to refine the structure to R/R_{free} of 16%/19%. Moreover, using EDEN it was also shown that there are two side chain conformations of Cys95 depending on which of two ruthenium complexes is bound to Adx (Figures 2.2.9.3.C and 2.2.9.3.D).

The "shuttle" mechanism of the electron transport by the ruthenium(II) bipyridyl complex-modified bovine adrenodoxin in the steroid hydroxylase: Crystal structure and intramolecular electron transfer

78

Figure 2.2.9.3 EDEN refinement of the electron density. A. The $2F_o$-F_c electron density at 0.8σ. The Δ-isomer (magenta) of the ruthenium(II) bipyridyl complex is shown only. B. EDEN density at 2.1σ. C. $2F_o$-F_c (blue), positive F_o-F_c (green), and negative F_o-F_c (red) electron densities generated with FFT. D. Generation of the electron density (yellow) using the EDEN formalism with properties of the omit map (blue $2F_o$-F_c).

The Ramachandran diagram shows that 95% of the amino-acid residues are in the most favored regions and almost 5% in additional allowed regions (Figure 2.2.9.4).
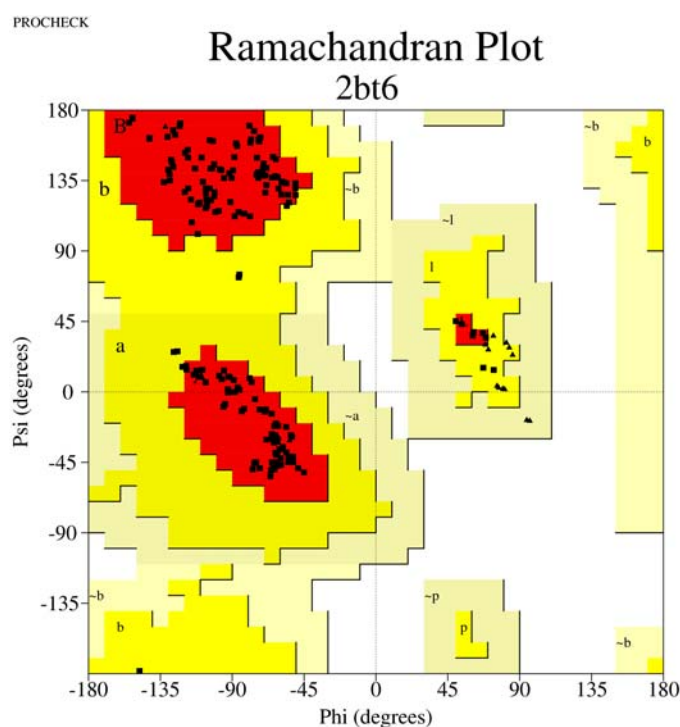
Figure 2.2.9.4 The Ramachandran plot. The picture was obtained after validation of the final refined structure of Ru(bpy)$_2$(mbpy)-Adx(1-108) running PROCHECK [Laskowski et al., 1993; Morris et al., 1992].

Andrei S. Halavaty, 2005

Adx(1-108) as well as Adx(4-108) consist of two structural domains (Figure 1.1.2.1.2). In general, there were no differences in the structure of both adrenodoxins. Fitting a subset of C^α positions of Ru(bpy)$_2$(mbpy)-Adx(1-108) onto the unmodified oxidized Adx(4-108) showed that the coupling of adrenodoxin with the bipyridyl complex did not influence the overall structure of Adx(1-108) (Figure 2.2.9.5). The backbone of the superimposed area (residues 6-108) of modified Adx(1-108) and unmodified Adx(4-108) is very similar with a root-mean-square deviation (r.m.s.d.) of 0.337 Å. Two Ru(bpy)$_2$(mbpy)-Adx(1-108) complexes and two Adx(4-108) molecules in their asymmetric units were also compared. The r.m.s.d. of C^α positions between two Ru(bpy)$_2$(mbpy)-Adx(1-108) was 0.150 Å, lower than that between two Adx(4-108) molecules, 0.428 Å, possibly reflecting lower resolution of the former structure. When superimposing each structure of oxidized Adx with the structure of the reduced full-length form, one difference in the region of the interaction F-helix was observed (Figure 2.2.9.5). Upon reduction this helix is moved away from its position in the oxidized protein, as determined by NMR [Beilke et al., 2002].

Average B/2 values were calculated for 1CJE as 533 Å (chainA-chainB interface) and 504 Å (chainC-chainD interface); for 1AYF as 372 Å (chainA-chainB interface); and for 2BT6 as 328 Å (chainA-chainB interface).
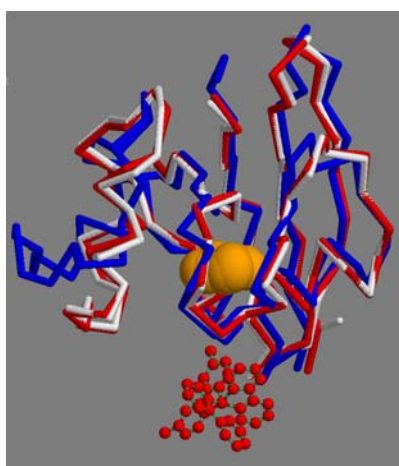
Figure 2.2.9.5 Superposition of C^α atoms of oxidized Ru(bpy)$_2$(mbpy)-Adx(1-108) (red), oxidized (white) and reduced (blue) full-length Adx structures. The [2Fe-2S] cluster of the ferredoxins is drawn with yellow-orange spheres. Ru(bpy)$_2$(mbpy) covalently bound to Cys95 of Adx(1-108) is drawn in red ball-and-stick representation. Picture generated by MOLMOL [Koradi et al., 1996].

Covalently bound Ru(bpy)$_2$(mbpy) is situated on the protein surface and tilted toward the [2Fe-2S] cluster (Figure 2.2.9.6.A). Two different possible intramolecular electron-transfer pathways were predicted by the program HARLEM for the two complexes in the asymmetric unit. Upon light absorption, an electron in the ruthenium complex is formally transferred from the excited metal center to one of the bipyridyl ligands, so that a metal-to-ligand charge-transfer state is formed. From the excited MLCT state of Ru(bpy)$_2$(mbpy), an electron will further be transferred to the Fe2 atom of the iron-sulfur cluster of Adx(1-108).
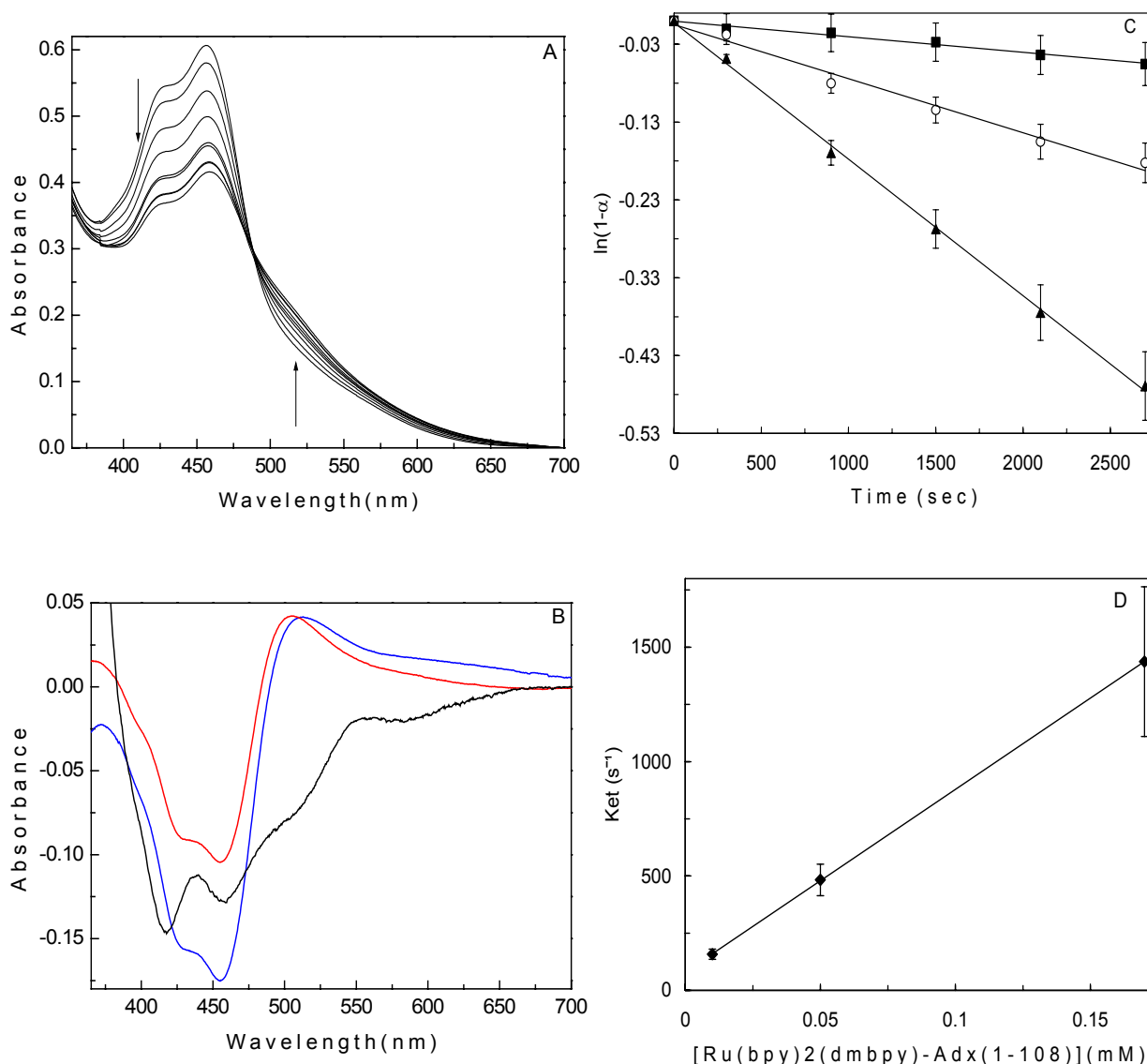
Andrei S. Halavaty, 2005
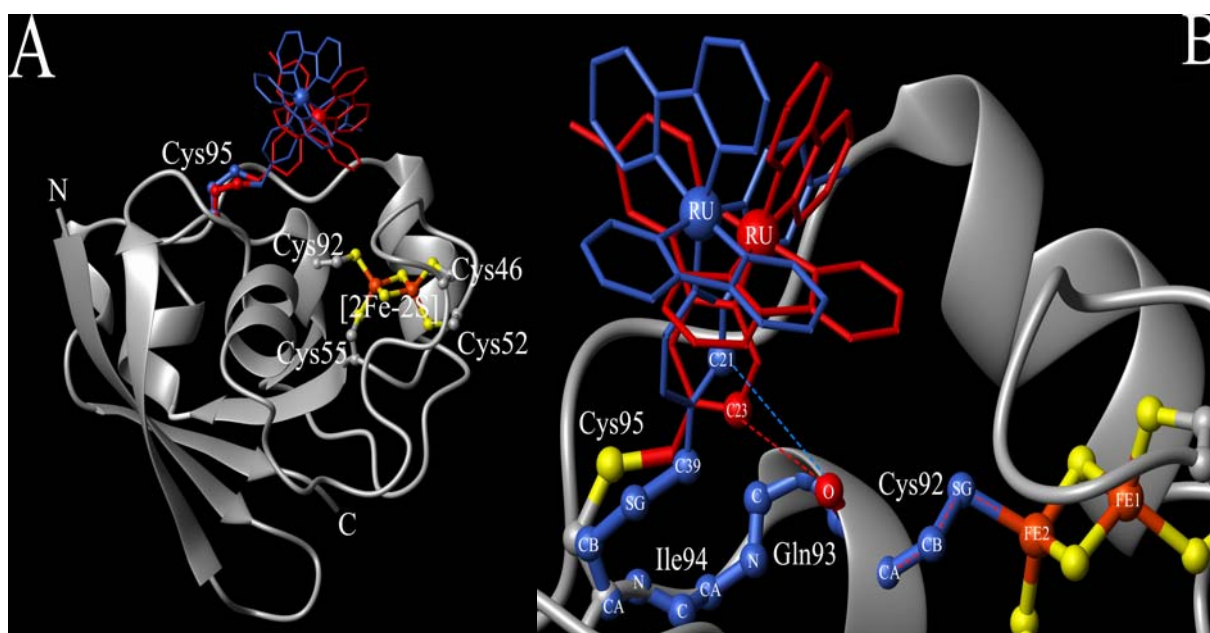
Figure 2.2.9.6 Molecular structure of Ru(bpy)$_2$(mbpy)-Adx(1-108). A. Secondary structure plot of the complex (molecule A). Ru(bpy)$_2$(mbpy) isomers are in stick representation (Λ - blue and Δ - red) with the ruthenium atoms as spheres. Cysteine side chains and the [2Fe-2S] cluster are drawn in ball-and-stick representation. B. Possible electron-transfer pathways calculated by the program HARLEM. Red dotted line – pathway for the Δ-isomer in molecule A and B. Through-space jump from the C^{21} atom of Ru(bpy)$_2$(mbpy) to the carbonyl O of Cys92 (Λ-isomer in molecule A), marked as a blue dotted line, is followed by further transfer through covalent bonds of Cys92 (marked also as red dotted line) as in the Δ-isomer. The path *via* the protein backbone is shown in blue ball-and-stick representation, starting from C^{39} of Ru(bpy)$_2$(mbpy). Pictures of the structure were prepared using the program MOLMOL [Koradi et al., 1996].

The first pathway is common to the Δ-isomers of Ru(bpy)$_2$(mbpy) bound to the molecules A (11.77 Å) and B (11.95 Å), and for the Λ-configuration in molecule A (12.62 Å) (Figure 2.2.9.6.B) and begins with a through-space jump from the C^{23} or C^{21} atom of the π-system of the MLCT to the carbonyl oxygen of Cys92. The further path leads *via* the covalent bonds of Cys92 to the Fe2 atom. The second path (23.71 Å) for the Λ-isomer in molecule B is longer and leads from C^{39} of the compound *via* the covalent bonds of the Cys95, Ile94, Gln93, and Cys92 residues to the Fe2 atom (Figure 2.2.9.6.B).

2.2.10 Light-induced reduction of the [2Fe-2S] cluster of Adx(1-108)

Illumination of Adx(1-108) did not affect its stability as proven by an unchanged absorption spectrum (data are not shown). For Ru(bpy)$_2$(mbpy)-Adx(1-108) a 30–40% absorbance decrease at 414 nm has been observed after 45 min of illumination (Figure

The "shuttle" mechanism of the electron transport by the ruthenium(II) bipyridyl complex-modified bovine adrenodoxin in the steroid hydroxylase: Crystal structure and intramolecular electron transfer

81

2.2.10.1.A). During irradiation of a Ru(bpy)$_2$(mbpy)-Adx(1-108) sample, a progressive absorbance increase between 487 nm and 700 nm was detectable with an isosbestic point at 487.5 nm (Figure 2.2.10.1.A). With every new illumination, this shoulder was getting more pronounced, and it influenced the shape of the difference spectra of Ru(bpy)$_2$(mbpy)-Adx(1-108). In Figure 2.2.10.1.B there is a prominent maximum at 500 nm in the difference spectrum of the photoreduced Ru(bpy)$_2$(mbpy)-Adx(1-108), which becomes a minimum in the chemically reduced Adx(1-108). On the other hand, coupled Adx(1-108) does not have a positive peak at 550 nm, whereas Adx(1-108) does. Addition of sodium dithionite to the Ru(bpy)$_2$(mbpy)-Adx(1-108) sample, after and during illumination, caused its final reduced and difference spectra to became comparable with those of the Na$_2$S$_2$O$_4$-reduced Adx(1-108) (data are not sown). 20–25% of the reoxidized Adx(1-108) was recovered after photoreduction.

The "shuttle" mechanism of the electron transport by the ruthenium(II) bipyridyl complex-modified bovine
adrenodoxin in the steroid hydroxylase: Crystal structure and intramolecular electron transfer

82

Figure 2.2.10.1 Photoreduction of Adx(1-108). A. Absorption spectra of oxidized and photoreduced (from the 15th to 75th minute) 1:1 Ru(bpy)$_2$(mbpy)-Adx(1-108) were obtained under anaerobic conditions. Downward and upward arrows indicate absorbance decrease at 414 nm and increase between 487 nm and 700 nm, respectively. B. The difference spectra of the photoreduced Ru(bpy)$_2$(mbpy)-Adx(1-108) after 15 (red) and 75 min (blue), and chemically reduced Adx(1-108) (black). C. Formation of photoreduced Ru(bpy)$_2$(mbpy)-Adx(1-108) as a function of the illumination time. Solid lines are linear fits of the function $ln(1-\alpha) = -k_{obs}t$ at 0.01 mM (■), 0.05 mM (○), and 0.17 mM (▲) of the Ru(bpy)$_2$(mbpy)-Adx(1-108) complex, respectively. Error bars correspond to relative errors of the reduced fraction $|\Delta\alpha/\alpha|$ of 50.5% (0.01 mM), 11.8% (0.05 mM), and 7.7% (0.17 mM) at 2700 s. D. Plot of k_{et} *versus* Ru(bpy)$_2$(mbpy)-Adx(1-108) concentrations (♦). Error bars correspond to the confidence intervals with significance level equals 0.05.

The "shuttle" mechanism of the electron transport by the ruthenium(II) bipyridyl complex-modified bovine adrenodoxin in the steroid hydroxylase: Crystal structure and intramolecular electron transfer

83

A linear relationship between $ln(1-\alpha)$ and t was observed (Figure 2.2.10.1.C). After 45 min data deviated from linearity and were, therefore, not included in the plot. Calculated k_{obs} are $(2.0\pm0.03)\times10^{-5}$ s^{-1} (0.01 mM), $(6.4\pm0.1)\times10^{-5}$ s^{-1} (0.05 mM), and $(1.8\pm0.2)\times10^{-4}$ s^{-1} (0.17 mM), where errors are the standard deviation from the linear fit (Figure 2.2.10.1.C). These rates were used to calculate the rates k_{et}, which are 158 ± 22 s^{-1} (0.01 mM), 483 ± 69 s^{-1} (0.05 mM), and 1437 ± 327 s^{-1} (0.17 mM). From the slope of the plot k_{et} $versus$ the Ru(bpy)$_2$(mbpy)-Adx(1-108) concentration (Figure 2.2.10.1.D) the intermolecular bimolecular rate constant k_{et2} = $(7.98\pm0.04)\times10^6$ M^{-1} s^{-1} was obtained. The y intercept of the linear fit at zero concentration of Ru(bpy)$_2$(mbpy)-Adx(1-108) gives the k_{et1} of (80.6 ± 3.6) s^{-1}.

In order to prove the light-induced reduction of the [2Fe-2S] cluster of Adx(1-108), EPR measurements after irradiation of the Ru(bpy)$_2$(mbpy)-Adx(1-108) sample were performed.

2.2.11 EPR data

In oxidized Adx(1-108), the iron-sulfur cluster is in the EPR silent [2Fe-2S]$^{2+}$ state. In this state the electron spins on both Fe^{III} irons (each S=5/2) couple antiferromagnetically to a total spin S = 0. In contrast, the reduced form, [2Fe-2S]$^{1+}$, in which the spins of Fe^{III} (S=5/2) and Fe^{II} (S=2) on both irons couple to a total electron spin S = ½, is EPR active. Illuminated unmodified Adx(1-108), and a 1:1 mixture of Adx(1-108) plus Ru(bpy)$_3$ showed no EPR signals characteristic for the reduced [2Fe-2S] cluster, indicating that the iron-sulfur cluster stays oxidized in the samples. In contrast, the EPR signal of the (photo)reduced iron-sulfur cluster of Adx(1-108) was obtained. Two traces, a and b in Figure 2.2.11.1, show that by dithionite reduction of Adx(1-108) two different species of the reduced [2Fe-2S] center were obtained. The first species exhibits a broader spectrum and g-values of $g_\parallel$ = 2.024(2) and $g_\perp$ = 1.938(2), which are in excellent agreement with values reported earlier [Tuckey et al., 2001]. In the trace b the low-field absorption line moved to higher field (lower g) and the high-field absorption moved to lower field (higher g) indicating perturbation at the site of the iron chromophore; calculated g-values are $g_\parallel$ = 2.012(2) and $g\perp$ = 1.942(2), respectively. The second species represents probably a small structural perturbation in the vicinity of the [2Fe-2S] cluster. The [2Fe-2S] cluster is situated near the protein surface, and small structural changes could be induced by different pH values, dithionite concentrations. The chemically reduced Ru(bpy)$_2$(mbpy)-Adx(1-108) sample (trace c in Figure 2.2.11.1) represents a superposition of the EPR spectra of the two above

The "shuttle" mechanism of the electron transport by the ruthenium(II) bipyridyl complex-modified bovine adrenodoxin in the steroid hydroxylase: Crystal structure and intramolecular electron transfer

84

species. Trace d in Figure 2.2.11.1 shows the EPR spectrum of the photoreduced [2Fe-2S] cluster in the Ru(bpy)$_2$(mbpy)-Adx(1-108) sample after 20 min of illumination, which is virtually identical with chemically reduced Adx(1-108) (trace a).

By spin quantification of the chemically reduced Adx(1-108) samples we have determined that the ratio between the concentration of spins and Adx(1-108) concentration was 1.09 and 1.1 in two independent measurements with an error of $\pm$ 10%. These results indicate that only one of two iron atoms in the iron-sulfur cluster is in the Fe^{2+} state, i.e. $[2Fe-2S]^{1+}$ state.
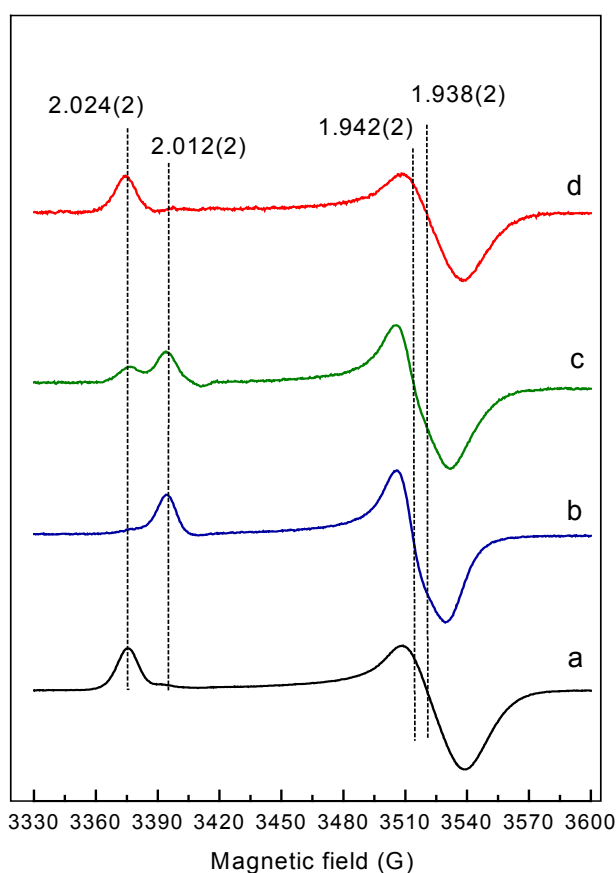
Figure 2.2.11.1 EPR spectra of the (photo)reduced [2Fe-2S] cluster of Adx(1-108). Trace a and b are EPR spectra of chemically reduced iron-sulfur cluster of Adx(1-108). Trace c is the EPR spectrum of dithionite-reduced cluster of Ru(bpy)$_2$(mbpy)-Adx(1-108). Trace d – EPR spectrum of the photoreduced [2Fe-2S] cluster of Ru(bpy)$_2$(mbpy)-Adx(1-108).

To summarize the present results of this PhD thesis one should say that the aimed photoreduction of the [2Fe-2S] cluster of bovine adrenodoxin *via* covalently attached on the protein surface ruthenium(II) bipyridyl complex is possible. Based on the 3D structure of the Ru(bpy)$_2$(mbpy)-Adx(1-108) complex, possible intramolecular electron-transfer pathways were proposed. Additionally, an unusual feature of Adx, an one-electron-carrier protein, to accept two electrons from an external reducing agent was observed.